10024 *Inorg. Chem.* **2009**, *48*, 10024–10035
DOI: 10.1021/ic9006668

Inorganic Chemistry
Article

A Hydrogen-Bond Facilitated Cycle for Oxygen Reduction by an Acid- and Base-Compatible Iron Platform

Han Sen Soo,[†,∥] Alexis C. Komor,[†] Anthony T. Iavarone,[§] and Christopher J. Chang*[,†,‡,∥]

[†]*Department of Chemistry,* [§]*QB3/Chemistry Mass Spectrometry Facility, and the* [‡]*Howard Hughes Medical Institute, University of California, Berkeley, California 94720, and* [∥]*Chemical Sciences Division, Lawrence Berkeley National Laboratory, Berkeley, California 94720*

Received April 5, 2009

We report a hydrogen-bond functionalized N4Py ligand platform (*N*,*N*-bis(2-R-6-pyridylmethyl)-*N*-bis(2-pyridyl)methylamine; R = neopentyl-NH, N4Py^{2NpNH}, **9**; R = phenyl-NH, N4Py^{2PhNH}, **10**) and the ability of its iron(II)-triflate [N4Py^{2R}Fe^{II}(OTf)][OTf] complexes (R = NpNH, **11**; R = PhNH, **12**) to activate and reduce dioxygen in a synthetic cycle by coupled proton and electron transfer. A pair of iron(III)-hydroxide [N4Py^{2R}Fe^{III}(OH)][OTf]$_2$ complexes (R = NpNH, **13**; R = PhNH, **14**) are isolated and structurally and spectroscopically characterized after exposure of the iron(II)-triflate precursors to 1 atm of O_2 at ambient temperature. The stability of this system to acids and bases allows regeneration of the labile iron(II)-triflate starting materials by sequential electron and proton transfer with cobaltocene and triflic acid, respectively, or through direct proton-coupled reduction with ascorbic acid. In the stepwise process, reduction of the iron(III)-hydroxide complexes with cobaltocene gives structurally homologous iron(II)-hydroxide [N4Py^{2R}Fe^{II}(OH)][OTf] congeners (R = NpNH, **15**; R = PhNH, **16**) that can be prepared independently from **11** and **12** with 20% aq. NaOH. Additions of triflic acid to complexes **15** and **16** furnish the starting compounds **11** and **12**, respectively, to complete the synthetic cycle. The combined data establish a synthetic cycle for O_2 reduction by an iron platform that manages proton and electron transfer through its first and second coordination spheres.

Introduction

Living systems exert exquisite control over first- and second-sphere coordination chemistry to direct reactivity at metal ion centers. Prominent examples include heme and non-heme enzymes that bind and activate dioxygen for a variety of functions by combining primary iron ligand fields with defined networks of secondary hydrogen-bond interactions.[1−9] Both monoiron and diiron intermediates have been invoked in O_2 activation and reduction cycles through coupled delivery of proton and electron equivalents to give

*To whom correspondence should be addressed. E-mail: chrischang@berkeley.edu.

(1) Baik, M. H.; Newcomb, M.; Friesner, R. A.; Lippard, S. J. *Chem. Rev.* **2003**, *103*, 2385–2420.
(2) Costas, M.; Mehn, M. P.; Jensen, M. P.; Que, L. *Chem. Rev.* **2004**, *104*, 939–986.
(3) Green, M. T.; Dawson, J. H.; Gray, H. B. *Science* **2004**, *304*, 1653–1656.
(4) Groves, J. T. *J. Inorg. Biochem.* **2006**, *100*, 434–447.
(5) Holm, R. H.; Kennepohl, P.; Solomon, E. I. *Chem. Rev.* **1996**, *96*, 2239–2314.
(6) Kovacs, J. A. *Chem. Rev.* **2004**, *104*, 825–848.
(7) Krebs, C.; Galonic Fujimori, D.; Walsh, C. T.; Bollinger, J. *Acc. Chem. Res.* **2007**, *40*, 484–492.
(8) Sono, M.; Roach, M. P.; Coulter, E. D.; Dawson, J. H. *Chem. Rev.* **1996**, *96*, 2841–2888.
(9) Williams, N. H.; Takasaki, B.; Wall, M.; Chin, J. *Acc. Chem. Res.* **1999**, *32*, 485–493.
(10) Babcock, G. T. *Proc. Natl. Acad. Sci. U.S.A.* **1999**, *96*, 12971–12973.
(11) Babcock, G. T.; Varotsis, C. *J. Bioenerg. Biomembr.* **1993**, *25*, 71–80.
(12) Blair, D. F.; Witt, S. N.; Chan, S. I. *J. Am. Chem. Soc.* **1985**, *107*, 7389–7399.
(13) Boulatov, R.; Collman, J. P.; Shiryaeva, I. M.; Sunderland, C. J. *J. Am. Chem. Soc.* **2002**, *124*, 11923–11935.
(14) Collman, J. P.; Devaraj, N. K.; Decreau, R. A.; Yang, Y.; Yan, Y. L.; Ebina, W.; Eberspacher, T. A.; Chidsey, C. E. D. *Science* **2007**, *315*, 1565–1568.
(15) Han, S.; Ching, Y.; Rousseau, D. L. *Nature* **1990**, *348*, 89–90.
(16) Han, S.; Ching, Y. C.; Rousseau, D. L. *J. Am. Chem. Soc.* **1990**, *112*, 9445–9451.
(17) Han, S. W.; Ching, Y. C.; Rousseau, D. L. *J. Biol. Chem.* **1989**, *264*, 6604–6607.
(18) Han, S. W.; Ching, Y. C.; Rousseau, D. L. *Proc. Natl. Acad. Sci. U.S.A.* **1990**, *87*, 2491–2495.
(19) Hill, B. C. *J. Biol. Chem.* **1994**, *269*, 2419–2425.
(20) Ji, H.; Yeh, S.-R.; Rousseau, D. L. *FEBS Lett.* **2005**, *579*, 6361–6364.
(21) Kim, S. O.; Sastri, C. V.; Seo, M. S.; Kim, J.; Nam, W. *J. Am. Chem. Soc.* **2005**, *127*, 4178–4179.
(22) Larsen, R. W.; Li, W.; Copeland, R. A.; Witt, S. N.; Lou, B. S.; Chan, S. I.; Ondrias, M. R. *Biochemistry* **1990**, *29*, 10135–10140.
(23) Lee, Y.-M.; Dhuri, S. N.; Sawant, S. C.; Cho, J.; Kubo, M.; Ogura, T.; Fukuzumi, S.; Nam, W. *Angew. Chem., Int. Ed.* **2009**, *48*, 1803–1806.
(24) MacBeth, C. E.; Golombek, A. P.; Young, V. G.; Yang, C.; Kuczera, K.; Hendrich, M. P.; Borovik, A. S. *Science* **2000**, *289*, 938–941.
(25) Proshlyakov, D. A.; Pressler, M. A.; Babcock, G. T. *Proc. Natl. Acad. Sci. U.S.A.* **1998**, *95*, 8020–8025.
(26) Que, L. *Acc. Chem. Res.* **2007**, *40*, 493–500.
(27) Shook, R. L.; Borovik, A. S. *Chem. Commun.* **2008**, *2008*, 6095–6107.
(28) Traylor, T. G.; Traylor, P. S. *Active Oxygen in Biochemistry*; Valentine, J. S., Foote, C. S., Liebman, J., Greenberg, A., Eds.; Blackie Academic and Professional, Chapman and Hall: London, U.K., 1995; pp 84−187.
(29) Varotsis, C.; Zhang, Y.; Appelman, E. H.; Babcock, G. T. *Proc. Natl. Acad. Sci. U.S.A.* **1993**, *90*, 237–241.

Published on Web 09/25/2009

iron oxo, hydroxo, and aquo species that ligate oxygen in a formally reduced O^{2-} state.[1,2,8,10−30]

Elucidating structure−activity relationships between metal centers and peripheral hydrogen bonds continues to motivate the creation of synthetic systems that combine primary- and secondary-sphere functionalities.[9,27,31−37] Of particular significance to iron−oxygen chemistry is pioneering work by Borovik, in which he utilized hydrogen-bond motifs to prepare and characterize anionic iron(III)-oxo and iron(III)/(II)-hydroxide complexes directly from oxygen or water.[24,31,38−49] Complementary breakthroughs in the preparation and evaluation of cationic iron(IV)-oxo and anionic iron(V)-oxo complexes by first-sphere approaches have been reported by Wieghardt,[50,51] Que,[2,26,52−76] Nam,[21,23,61,72,74,77−79] Collins,[80] and others;[58,62,67−71,81−84] some of these latter iron(IV)-oxo systems have been accessed via oxygen or water using ethereal/alcohol solvents or other additives.[21,23,26] In addition, Collman and Chidsey have prepared and studied functional cytochrome *c* oxidase models that faithfully reduce O_2 directly to H_2O.[13,14,85]

We have initiated a program aimed at influencing inorganic small-molecule activation chemistry by the addition of second-sphere functionalities, focusing on iron and other earth-abundant metals.[86,87] In this report, we present a new N4Py platform that incorporates hydrogen-bonding and the ability of its iron(II) complexes to activate and reduce O_2 in a synthetic cycle by dual proton and electron transfer. This system is distinguished from other hydrogen-bonded cavities by its stability to strong acids and bases, allowing synthetic isolation and structural characterization of homologous iron(III)- and iron(II)-hydroxide intermediates and their

(30) Varotsis, C. A.; Babcock, G. T. *J. Am. Chem. Soc.* **1995**, *117*, 11260–11269.
(31) Borovik, A. S. *Acc. Chem. Res.* **2005**, *38*, 54–61.
(32) Chang, C. J.; Chng, L. L.; Nocera, D. G. *J. Am. Chem. Soc.* **2003**, *125*, 1866–1876.
(33) Makowska-Grzyska, M. M.; Jeppson, P. C.; Allred, R. A.; Arif, A. M.; Berreau, L. M. *Inorg. Chem.* **2002**, *41*, 4872–4887.
(34) Mareque-Rivas, J. C.; Prabaharan, R.; Parsons, S. *Dalton Trans.* **2004**, 1648–1655.
(35) Natale, D.; Mareque-Rivas, J. C. *Chem. Commun.* **2008**, 425–437.
(36) Rosenthal, J.; Nocera, D. *Acc. Chem. Res.* **2007**, *40*, 543–553.
(37) Wada, A.; Honda, Y.; Yamaguchi, S.; Nagatomo, S.; Kitagawa, T.; Jitsukawa, K.; Masuda, H. *Inorg. Chem.* **2004**, *43*, 5725–5735.
(38) Dey, A.; Hocking, R. K.; Larsen, P.; Borovik, A. S.; Hodgson, K. O.; Hedman, B.; Solomon, E. I. *J. Am. Chem. Soc.* **2006**, *128*, 9825–9833.
(39) Gupta, R.; Borovik, A. S. *J. Am. Chem. Soc.* **2003**, *125*, 13234–13242.
(40) Lucas, R. L.; Powell, D. R.; Borovik, A. S. *J. Am. Chem. Soc.* **2005**, *127*, 11596–11597.
(41) Lucas, R. L.; Zart, M. K.; Murkerjee, J.; Sorrell, T. N.; Powell, D. R.; Borovik, A. S. *J. Am. Chem. Soc.* **2006**, *128*, 15476–15489.
(42) MacBeth, C. E.; Gupta, R.; Mitchell-Koch, K. R.; Young, V. G.; Lushington, G. H.; Thompson, W. H.; Hendrich, M. P.; Borovik, A. S. *J. Am. Chem. Soc.* **2004**, *126*, 2556–2567.
(43) MacBeth, C. E.; Hammes, B. S.; Young, V. G.; Borovik, A. S. *Inorg. Chem.* **2001**, *40*, 4733–4741.
(44) Mukherjee, J.; Lucas, R. L.; Zart, M. K.; Powell, D. R.; Day, V. W.; Borovik, A. S. *Inorg. Chem.* **2008**, *47*, 5780–5786.
(45) Parsell, T. H.; Yang, M.-Y.; Borovik, A. S. *J. Am. Chem. Soc.* **2009**, *131*, 2762–2763.
(46) Zinn, P. J.; Sorrell, T. N.; Powell, D. R.; Day, V. W.; Borovik, A. S. *Inorg. Chem.* **2007**, *46*, 10120–10132.
(47) Larsen, P. L.; Gupta, R.; Powell, D. R.; Borovik, A. S. *J. Am. Chem. Soc.* **2004**, *126*, 6522–6523.
(48) Shirin, Z.; Hammes, B. S.; Young, V. G.; Borovik, A. S. *J. Am. Chem. Soc.* **2000**, *122*, 1836–1837.
(49) Zart, M. K.; Powell, D.; Borovik, A. S. *Inorg. Chim. Acta* **2007**, *360*, 2397–2402.
(50) Berry, J. F.; Bill, E.; Bothe, E.; George, S. D.; Mienert, B.; Neese, F.; Wieghardt, K. *Science* **2006**, *312*, 1937–1941.
(51) Grapperhaus, C. A.; Mienert, B.; Bill, E.; Weyhermuller, T.; Wieghardt, K. *Inorg. Chem.* **2000**, *39*, 5306–5317.
(52) Bassan, A.; Blomberg, M. R. A.; Siegbahn, P. E. M.; Que, L. J. *Angew. Chem., Int. Ed.* **2005**, *44*, 2939–2941.
(53) Bautz, J.; Bukowski, M. R.; Kerscher, M.; Stubna, M.; Comba, P.; Lienke, A.; Münck, E.; Que, L. J. *Angew. Chem., Int. Ed.* **2006**, *45*, 5681–5684.
(54) Bell, C. B. I.; Wong, S. D.; Xiao, Y.; Klinker, E. J.; Tenderholt, A. L.; Smith, M. C.; Rohde, J.-U.; Que, L. J.; Cramer, S. P.; Solomon, E. I. *Angew. Chem., Int. Ed.* **2008**, *47*, 9071–9074.
(55) Chavez, F. A.; Ho, R. Y. N.; Pink, M.; Young, V. G. J.; Kryatov, S. V.; Rybak-Akimova, E. V.; Andres, H.; Münck, E.; Que, L. J.; Tolman, W. B. *Angew. Chem., Int. Ed.* **2002**, *41*, 149–152.
(56) Dong, Y.; Yan, S.; Young, V. G. J.; Que, L. J. *Angew. Chem., Int. Ed. Engl.* **1996**, *35*, 618–620.
(57) Emerson, J. P.; Farquhar, E. R.; Que, L. J. *Angew. Chem., Int. Ed.* **2007**, *46*, 8553–8556.
(58) Ho, R. Y. N.; Roelfes, G.; Feringa, B. L.; Que, L. *J. Am. Chem. Soc.* **1999**, *121*, 264–265.
(59) Kaizer, J.; Costas, M.; Que, L. J. *Angew. Chem., Int. Ed.* **2003**, *42*, 3671–3673.
(60) Klinker, E. J.; Kaizer, J.; Brennessel, W. W.; Woodrum, N. L.; Cramer, C. J.; Que, L. J. *Angew. Chem., Int. Ed.* **2005**, *44*, 3690–3694.
(61) Lim, M. H.; Rohde, J.-U.; Stubna, A.; Bukowski, M. R.; Costas, M.; Ho, R. Y. N.; Münck, E.; Nam, W.; Que, L. *Proc. Natl. Acad. Sci. U.S.A.* **2003**, *100*, 3665–3670.
(62) Lubben, M.; Meetsma, A.; Wilkinson, E. C.; Feringa, B.; Que, L. J. *Angew. Chem., Int. Ed. Engl.* **1995**, *34*, 1512–1514.
(63) Oldenburg, P. D.; Ke, C.-Y.; Tipton, A. A.; Shteinman, A. A.; Que, L. J. *Angew. Chem., Int. Ed.* **2006**, *45*, 7975–7978.
(64) Pestovsky, O.; Stoian, S.; Bominaar, E. L.; Shan, X.; Münck, E.; Que, L. J.; Bakac, A. *Angew. Chem., Int. Ed.* **2005**, *44*, 6871–6874.
(65) Que, L.; Ho, R. Y. N. *Chem. Rev.* **1996**, *96*, 2607–2624.
(66) Ray, K.; England, J.; Fiedler, A. T.; Martinho, M.; Münck, E.; Que, L. J. *Angew. Chem., Int. Ed.* **2008**, *47*, 8068–8071.
(67) Roelfes, G.; Branum, M. E.; Wang, L.; Que, L.; Feringa, B. L. *J. Am. Chem. Soc.* **2000**, *122*, 11517–11518.
(68) Roelfes, G.; Hage, R.; Que, L.; Feringa, B. L. *J. Inorg. Biochem.* **1999**, *74*, 279–279.
(69) Roelfes, G.; Lubben, M.; Chen, K.; Ho, R. Y. N.; Meetsma, A.; Genseberger, S.; Hermant, R. M.; Hage, R.; Mandal, S. K.; Young, V. G.; Zang, Y.; Kooijman, H.; Spek, A. L.; Que, L.; Feringa, B. L. *Inorg. Chem.* **1999**, *38*, 1929–1936.
(70) Roelfes, G.; Lubben, M.; Hage, R.; Que, L.; Feringa, B. L. *Chem.—Eur. J.* **2000**, *6*, 2152–2159.
(71) Roelfes, G.; Vrajmasu, V.; Chen, K.; Ho, R. Y. N.; Rohde, J.-U.; Zondervan, C.; la Crois, R. M.; Schudde, E. P.; Lutz, M.; Spek, A. L.; Hage, R.; Feringa, B. L.; Munck, E.; Que, L. *Inorg. Chem.* **2003**, *42*, 2639–2653.
(72) Rohde, J.-U.; In, J.-H.; Lim, M. H.; Brennessel, W. W.; Bukowski, M. R.; Stubna, A.; Munck, E.; Nam, W.; Que, L., Jr. *Science* **2003**, *299*, 1037–1039.
(73) Rohde, J.-U.; Que, L. J. *Angew. Chem., Int. Ed.* **2005**, *44*, 2255–2258.
(74) Seo, M. S.; In, J.-H.; Ok, S.; Young, K. N.; Hong, J. O.; Kim, J.; Que, L. J.; Nam, W. *Angew. Chem., Int. Ed.* **2004**, *43*, 2417–2420.
(75) Shan, X.; Que, L. *Proc. Natl. Acad. Sci. U.S.A.* **2005**, *102*, 5340–5345.
(76) Zhou, Y.; Shan, X.; Mas-BallestÉ, R.; Bukowski, M. R.; Stubna, A.; Chakrabarti, M.; Slominski, L.; Halfen, J. A.; Münck, E.; Que, L. J. *Angew. Chem., Int. Ed.* **2008**, *47*, 1896–1899.
(77) Fukuzumi, S.; Kotani, H.; Lee, Y.-M.; Nam, W. *J. Am. Chem. Soc.* **2008**, *130*, 15134–15142.
(78) Nam, W. *Acc. Chem. Res.* **2007**, *40*, 522–531.
(79) Nam, W.; Choi, S. K.; Lim, M. H.; Rohde, J.-U.; Kim, I.; Kim, J.; Kim, C.; Que, L. J. *Angew. Chem., Int. Ed.* **2003**, *42*, 109–111.
(80) de Oliveira, F. T.; Chanda, A.; Banerjee, D.; Shan, X.; Mondal, S.; Que, L., Jr.; Bominaar, E. L.; Munck, E.; Collins, T. J. *Science* **2007**, *315*, 835–838.
(81) Martinho, M.; Banse, F.; Bartoli, J. F.; Mattioli, T. A.; Battioni, P.; Horner, O.; Bourcier, S.; Girerd, J. J. *Inorg. Chem.* **2005**, *44*, 9592–9596.
(82) Martinho, M.; Banse, F.; Sainton, J.; Philouze, C.; Guillot, R.; Blain, G.; Dorlet, P.; Lecomte, S.; Girerd, J.-J. *Inorg. Chem.* **2007**, *46*, 1709–1717.
(83) Thibon, A.; England, J.; Martinho, M.; Young, V. G. J.; Frisch, J. R.; Guillot, R.; Girerd, J.-J.; Münck, E.; Que, L. J.; Banse, F. *Angew. Chem., Int. Ed.* **2008**, *47*, 7064–7067.
(84) Vrajmasu, V.; Munck, E.; Ho, R.; Que, L.; Roefles, G.; Feringa, B. L. *J. Inorg. Biochem.* **2001**, *86*, 472–472.
(85) Collman, J. P.; Ghosh, S.; Dey, A.; Decreau, R. A.; Yang, Y. *J. Am. Chem. Soc.* **2009**, *131*, 5034–5035.
(86) Harman, W. H.; Chang, C. J. *J. Am. Chem. Soc.* **2007**, *129*, 15128–15129.
(87) Bigi, J. P.; Hanna, T. E.; Harman, W. H.; Chang, A. L.; Chang, C. J., *submitted for publication.*

conversion back to labile iron(II) precursors by controlled electron and proton transfer. Mass spectrometry and infrared absorption measurements with various isotope labels are consistent with inner-sphere O_2 activation and reduction by first- and second-sphere participation. The collective data establish a synthetic O_2 reduction cycle mediated by synergistic first- and second-sphere coordination chemistry.

Results and Discussion

Design, Synthesis, and Oxygen Reactivity of Hydrogen-Bonded Iron(II) N4Py^{2R} Complexes. Our initial approach to testing second-sphere effects on metal ion reactivity relies on modulating established metal sites by the addition of secondary hydrogen bonding. Inspired in the context of iron−oxygen chemistry by cationic iron(IV)-oxo species with polyamine/pyridine ligands produced by Wieghardt,[50,51] Que,[2,26,52−76,79,81−84] Nam,[21,23,74,77−79] and others,[58,62,67−71,80−84] as well as anionic hydrogen-bonded iron(III)-oxo and iron(II)/(III)-hydroxide complexes stabilized by Borovik's trianionic amide cavities,[24,27,31,38,39,41−44,49] we sought to create hybrid ligand systems that combine a neutral primary ligand sphere and a well-defined secondary hydrogen-bond architecture. We reasoned that pyridine-rich inner-sphere metal platforms with pendant amines would provide the acid and base stability necessary to facilitate O_2 activation, reduction, cleavage, and cycling by proton and electron additions.

To this end, we prepared two new N4Py-type ligand frameworks bearing second-sphere neopentyl amine or aniline groups as outlined in Scheme 1 (N4Py^{2R}; R = NpNH, **9**; PhNH, **10**). The pentadentate N4Py platform supports six-coordinate metal complexes with one exchangeable apical site, and the neopentyl amine and aniline hydrogen-bond pendants provide steric bulk as well as a comparison between aliphatic and aromatic amines. Related tripodal systems with secondary amides and amines have been reported to exhibit enhanced hydrolytic capabilities.[9,33−35,37,46] Using *N*-bromosuccinimide (NBS), the appropriate 6-substituted-2-picolines[82,88] (**1** and **3**) were subjected to free radical bromination conditions to give statistical mixtures of products, from which the monobrominated products[82] (**4** and **5**) were isolated by silica column chromatography. The N4Py^{2R} derivatives (**6** and **7**) are assembled at room temperature by combining di-2-pyridylmethanamine[89,90] with **4** and **5**, respectively, in the presence of cesium carbonate and sodium iodide. After acid hydrolysis of **6** to afford the primary amine **8**, reductive amination with pivaldehyde and sodium triacetoxyborohydride provides the ligand **9** as a white foamy material after aqueous workup. Acid deprotection of **7** to remove the *tert*-butyloxycarbonyl (Boc) group produces the ligand **10** as a white foamy material.

Metalations of **9** and **10** with $Fe(OTf)_2(CH_3CN)_2$ in ethereal or nitrile solvents at room temperature proceed smoothly to give the corresponding [N4Py^{2R} Fe^{II}(OTf)][OTf] complexes (R = NpNH, **11**; R = PhNH, **12**) in good yields as yellow crystalline materials (Scheme 2). Both congeners were identified and characterized by X-ray structural analyses (vide infra), ^{1}H NMR spectroscopy, and elemental analyses. The addition of second-sphere hydrogen-bond groups markedly affects the structural and magnetic properties of the iron-N4Py platform. The complexes **11** and **12** each possesses an inner-sphere triflate anion as an axial ligand (vide infra), whereas the parent iron(II)-triflate complex [N4PyFe^{II}(CH$_3$CN)][OTf]$_2$ that lacks hydrogen-bond pendants binds an acetonitrile ligand at its apical sixth coordination site.[58,62,67−71,77,84] Moreover, ^{1}H NMR spectra indicate that the second-sphere functionalized iron(II)-triflates are paramagnetic, as opposed to the diamagnetic [N4PyFe^{II}(CH$_3$CN)][OTf]$_2$.[58,62,67−71,77,84] The effective magnetic moment values determined by the solution Evans' method for complexes **11** (μ_{eff} = 5.1) and **12** (μ_{eff} = 4.7) are indicative of high-spin iron(II) (S = 2) ground states, compared to the low-spin iron(II) (S = 0) ground state for the parent N4Py iron(II)-triflate complex.

The structural and electronic differences induced by second-sphere hydrogen bonding have patent consequences for O_2 reactivity. Whereas the parent (N4Py)Fe^{II} system is indefinitely stable to air,[62,67−71,84] exposure of 1 atm of O_2 to orange acetonitrile solutions of complexes **11** and **12** leads to clean formation of isolable dark blue [N4Py^{2R}Fe^{III}(OH)][OTf]$_2$ counterparts (R = NpNH, **13**; R = PhNH, **14**), as determined by X-ray structural (vide infra) and elemental analyses (Scheme 2). The monomeric iron(III)-hydroxide complexes can also be prepared using PhIO as the oxidant. Solution magnetic susceptibility measurements by the Evans' method are consistent with high-spin iron(III) (S = 5/2) products, and complex **13** was additionally identified by electrospray ionization (ESI) mass spectrometry. Because of the sterically encumbering and stabilizing hydrogen-bond pendants, we do not observe the Fe$^{III}_2$(μ-O) sinks that form during side reactions with the parent N4Py system.[69]

The second-sphere hydrogen-bond facilitated activation and cleavage of O_2 by this 4-fold symmetric, cationic iron(II) platform is complementary to Borovik's 3-fold symmetric, anionic iron(II) systems,[24,27,31,38−45,47−49,91] but a distinguishing feature of the cationic iron-N4Py^{2R} complexes reported here is their enhanced stability to both acids and bases. Because the generation of monomeric N4Py^{2R} iron(III)-hydroxide species from O_2 represents a formal reduction of substrate to the O^{2-} oxidation state, we sought to complete the synthetic cycle at the metal site by addition of electron and proton equivalents to regenerate the iron(II) starting material and release H_2O. Along these lines, cyclic voltammograms of **13** and **14** show reversible iron(III)/iron(II) reduction waves at 0 mV (**13**) and −210 mV (**14**) versus Fc$^+$/Fc (Figure 1). Treatment of the dark blue complexes **13** and **14** with cobaltocene generates their red iron(II)-hydroxide [N4Py^{2R}Fe^{II}(OH)][OTf] counterparts (R = NpNH, **15**; R = PhNH, **16**) as determined by X-ray structural (vide infra) and elemental analyses (Scheme 2). Both complexes were further characterized by ^{1}H NMR and IR spectroscopy, and the μ_{eff} values (μ_{eff} = 4.7, **15**; μ_{eff} = 4.6, **16**)

(88) Kadish, K. M.; Nguyen, M.; Van Caemelbecke, E.; Bear, J. L. *Inorg. Chem.* **2006**, *45*, 5996–6003.
(89) Chang, J.; Plummer, S.; Berman, E. S. F.; Striplin, D.; Blauch, D. *Inorg. Chem.* **2004**, *43*, 1735–1742.
(90) Renz, M.; Hemmert, C.; Meunier, B. *Eur. J. Org. Chem.* **1998**, 1271–1273.
(91) Shook, R. L.; Gunderson, W. A.; Greaves, J.; Ziller, J. W.; Hendrich, M. P.; Borovik, A. S. *J. Am. Chem. Soc.* **2008**, *130*, 8888–8889.

Scheme 1. Synthetic Scheme for Ligands **9** and **10** (Np = neopentyl; Ph = phenyl)

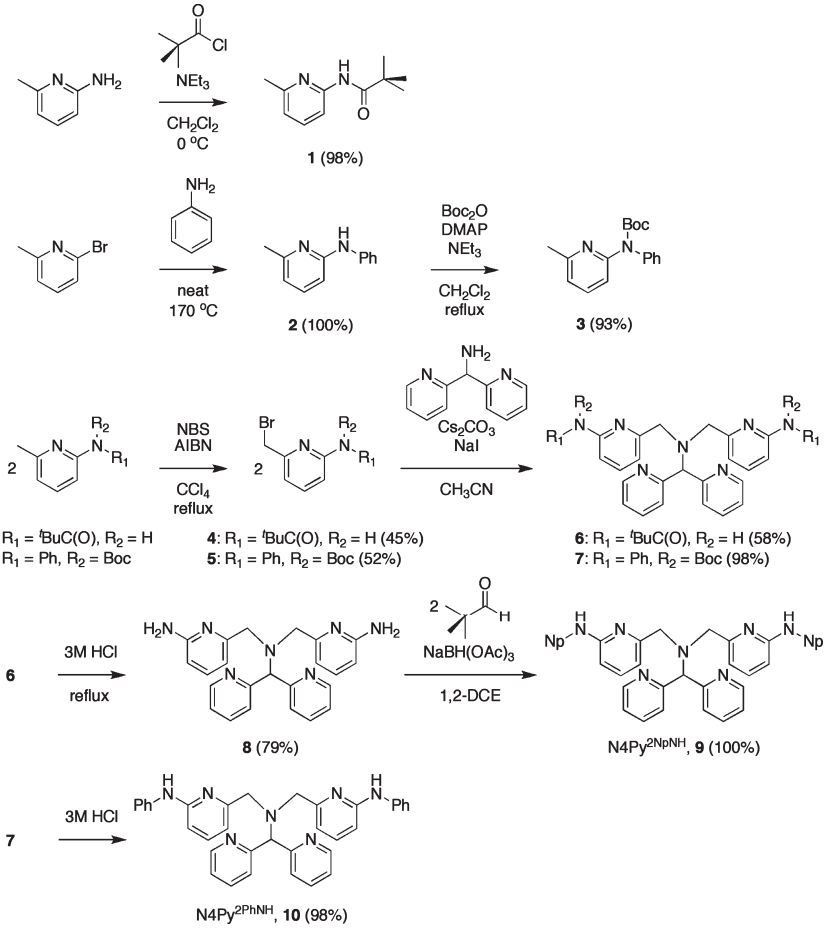

Scheme 2. Preparation and Reactivity of **11** and **12**

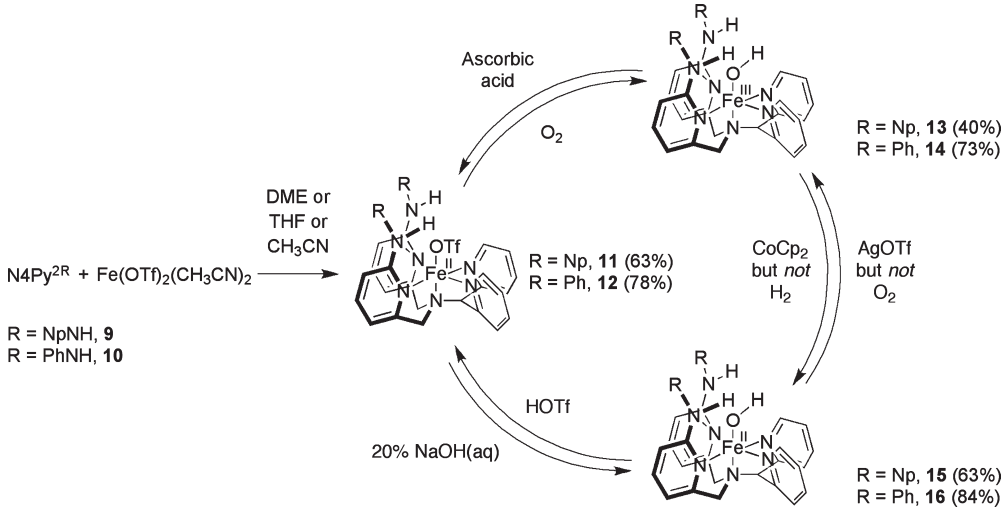

determined by the Evans' method in solution suggest high-spin iron(II) ($S = 2$) ground states. The monomeric $N4Py^{2R}$ iron(II)-hydroxide compounds can also be prepared independently by the reaction of **11** and **12** with 20% aq. NaOH, showing the stability of this system to bases. Furthermore, protonation of **15** and **16** with triflic acid regenerates the starting complexes **11** and **12**, respectively, as confirmed by ^{1}H NMR and UV−visible spectroscopy, establishing the acid stability of these hydrogen-bond cavities.[24,27,31,38−45,47−49,91] This stepwise addition of electron and proton equivalents closes the synthetic cycle for the full reduction of O_2 to the O^{2-} oxidation state with concomitant release of the labile iron(II)-triflate starting materials (Scheme 2). Alternatively, a direct and mild proton-coupled electron transfer reduction of **13** and **14** to **11** and **12**, respectively, can also be achieved by ascorbic acid (Scheme 2).[92]

(92) Warren, J. J.; Mayer, J. M. *J. Am. Chem. Soc.* **2008**, *130*, 7546–7547.

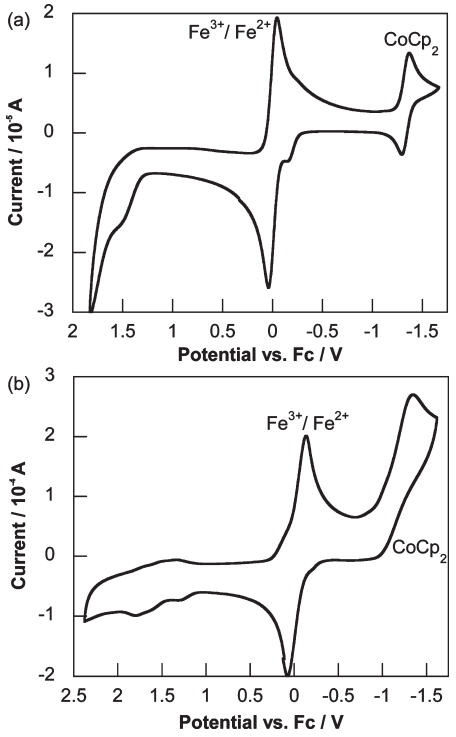

Figure 1. (a) Cyclic voltammogram for a 1 mM solution of **13** in CH_3CN, with the data collected using a glassy carbon electrode at a scan rate of 100 mV s^{-1}; the reversible reductive wave is at 0 V relative to ferrocene. (b) Cyclic voltammogram for a 1 mM solution of **14** in CH_3CN, with the data collected using a glassy carbon electrode at a scan rate of 100 mV s^{-1}; the reversible reductive wave is at −210 mV relative to ferrocene.

Control experiments were performed to rule out adventitious outer-sphere oxidation and aquation pathways and support an inner-sphere pathway. Cyclic voltammograms of the iron(II)-triflate complexes **11** and **12** show no oxidative waves within the acetonitrile solvent window (up to +1500 mV versus Fc^+/Fc, ferrocene, Supporting Information, Figure S1), which precludes outer-sphere oxidation. Indeed, exposing iron(II)-hydroxide complexes **15** and **16** to 1 atm of O_2 does not produce the corresponding oxidized iron(III)-hydroxide congeners **13** and **14**; in particular, compound **16** is indefinitely unreactive toward O_2. In addition, mass spectrometry studies using ^{18}O-labeled dioxygen show ^{18}O enrichment in the iron(III)-hydroxide product, consistent with inner-sphere chemistry (vide infra). Finally, to rule out adventitious free radical chain autoxidation pathways, reactions were carried out with 20 mM of **11** under 1.0 atm O_2 in the presence of 1 equiv of the radical chain quencher butylated hydroxytoluene (BHT). Rather than terminating or inhibiting the reaction, the observed initial rate for O_2 reduction was comparable with or without the BHT additive, suggesting that the activation of O_2 had not been quenched. Reactions showed clean isosbestic conversions of **11** to **13** at room temperature (Figure 2), with no observable intermediates.

Solid State Structures of Complexes 11− 14 and 16. Single-crystal X-ray analysis of compounds **11**−**14** and **16** provide solid-state structural snapshots of the hydrogen-bond facilitated cycle for oxygen reduction (Scheme 2). Crystallographic data are given in Table 1, and selected bond distances and angles are summarized in Table 2.

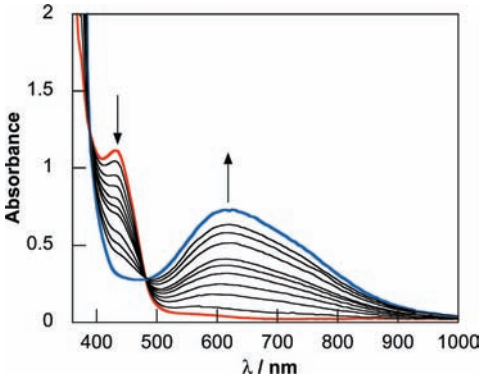

Figure 2. UV−visible absorption changes during the reaction of **11** and O_2 in CH_3CN at room temperature to generate **13**.

The molecular structures of **11**− **14** and **16** are shown in Figures 3 − 5 and Scheme 2.

Single crystals of **11** and **12** were obtained at room temperature as yellow blocks from 1,2-dimethoxyethane (DME) solutions layered beneath pentane. The complexes are isostructural but not isomorphous (Figure 3). Both **11** and **12** each possesses a triflate anion at the apical sixth site, as opposed to the parent $[N4PyFe^{II}(CH_3CN)][OTf]_2$ complex that possesses an axial coordinated acetonitrile ligand.[58,62,67−71,77,84] For both complexes **11** and **12**, the N7 amine and the O1 triflate atoms are closer than the van der Waal's radii for usual N−O distances and suggest the ability of these hydrogen-bonding cavities to stabilize electronegative, anionic ligands. The iron-ligand bonds for the second-sphere $N4Py^{2R}$ iron(II) complexes are also longer on average than those of the parent N4Py system, as anticipated for high spin $S = 2$ species compared to low spin $S = 0$ complexes.[58,62,67−71,77,84]

Single crystals of the isostructural **13** and **14** (Figure 4) were grown at −35 °C as dark blue blades from solutions of tetrahydrofuran (THF) or DME layered below solutions of diethyl ether (Et_2O) and pentane. These iron(III) complexes possess shorter metal−ligand bond distances than their corresponding iron(II)-triflate complexes because of higher effective nuclear charges for the former, but the observed differences are not large since oxidation from high-spin d^6 iron(II) to high-spin d^5 iron(III) in this ligand field removes an electron from a largely nonbonding d_{xy} orbital (Table 2). The $N4Py^{2R}$ Fe−OH distances of 1.837 Å (R = NpNH) and 1.835 Å (R = PhNH) are short but comparable to previously structurally characterized iron(III)-oxo and iron(III)-hydroxide units in synthetic[24,27,31,41,44,46,86,93,94] and biological systems.[95] Table 3 provides a comparison of Fe−O bond lengths for selected systems. Owing to hydrogen-bonding interactions, the observed O1−N5/N7 distances of 2.8 to 2.9 Å are shorter than typical van der Waal's distances (ca. 3.4 Å).

Finally, the reduced iron(II)-hydroxide complex **16** (Figure 5) was crystallized from THF/pentane mixtures. As anticipated, the inner-sphere metal−ligand bonds for

(93) Ogo, S.; Wada, S.; Watanabe, Y.; Iwase, M.; Wada, A.; Harata, M.; Jitsukawa, K.; Masuda, H.; Einaga, H. *Angew. Chem., Int. Ed.* **1998**, *37*, 2102–2104.
(94) Yeh, C. Y.; Chang, C. J.; Nocera, D. G. *J. Am. Chem. Soc.* **2001**, *123*, 1513–1514.
(95) Green, M. T. *J. Am. Chem. Soc.* **2006**, *128*, 1902–1906.

Table 1. Crystallographic Data for Complexes **11**−**14** and **16**

	11	**13**	**12**	**14**	**16**
chemical formula	$C_{35}H_{43}F_6FeN_7O_6S_2$	$C_{43}H_{60}F_6FeN_7O_9S_2$	$C_{39}H_{36}F_6FeN_7O_7S_2$	$C_{41}H_{42}F_6FeN_7O_9S_2$	$C_{148}H_{128}F_{12}Fe_4N_{29}O_{16}S_4$
formula weight	891.73	1052.95	948.72	1010.79	3148.47
T (K)	126	165	155	160	124
λ (Å)	0.71073	0.71073	0.71073	0.71073	0.71073
crystal system	triclinic	monoclinic	monoclinic	triclinic	triclinic
space group	$P\bar{1}$(No. 2)	$P2_1/n$ (No. 14)	$P2_1/c$ (No. 14)	$P\bar{1}$(No. 2)	$P\bar{1}$(No. 2)
a (Å)	9.8538(18)	9.9988(9)	10.2218(5)	12.0572(15)	12.2707(13)
b (Å)	11.491(2)	11.1928(10)	33.5162(17)	12.9077(16)	15.1201(16)
c (Å)	18.506(3)	44.421(4)	12.3587(6)	17.156(2)	20.548(2)
α (deg)	77.179(2)	90	90	69.948(2)	90.005(2)
β (deg)	77.311(2)	93.670(2)	104.229(1)	87.976(2)	101.953(2)
γ (deg)	80.914(2)	90	90	65.822(2)	109.126(2)
V (Å^3)	1980.2(6)	4961.2(8)	4104.1(4)	2258.8(5)	3514.3(6)
Z	2	4	4	2	1
ρ_{calcd} (g/cm^3)	1.496	1.410	1.535	1.486	1.489
μ(mm^{-1})	0.568	0.470	0.555	0.513	0.557
F(000)	924	2204	1948	1042	1624
reflctns collected	10073	27666	23326	14627	22767
ind reflctns (R_{int})	6477 (0.013)	10062 (0.033)	8381 (0.028)	9030 (0.017)	14048 (0.036)
T_{min}/T_{max}	0.89	0.88	0.88	0.83	0.89
data/restr/params	5205/0/514	7566/0/657	7034/92/609	6951/45/628	9861/4/978
R, R_{all}, wR_2	0.065, 0.080, 0.20	0.084, 0.011, 0.22	0.052, 0.063, 0.13	0.056, 0.073, 0.17	0.064, 0.096, 0.16
GOF	1.06	1.08	1.08	1.07	1.02
max shift/error	0.01	2.95	0.01	0.01	0.17

Table 2. Selected Bond Lengths (Å) and Angles for Complexes **11**−**14** and **16**

	11	**13**	**12**	**14**	**16**[a]
Fe1−O1	2.084(3)	1.837(3)	2.073(2)	1.835(2)	1.915(3)
Fe1−N1	2.180(3)	2.183(3)	2.179(2)	2.172(2)	2.236(3)
Fe1−N2	2.264(4)	2.160(4)	2.242(2)	2.138(2)	2.199(3)
Fe1−N3	2.171(3)	2.164(4)	2.187(2)	2.151(2)	2.204(4)
Fe1−N4	2.212(3)	2.119(4)	2.219(2)	2.132(2)	2.255(3)
Fe1−N6	2.243(3)	2.111(4)	2.227(2)	2.148(3)	2.221(3)
O1−(H5)−N5	3.352	2.865	3.356	2.867	2.782
O1−(H7)−N7	3.101	2.857	2.992	2.796	2.786
O1−Fe1−N1	168.96(13)	172.27(13)	165.79(9)	176.54(9)	177.05(13)

[a] Data taken from only one of two distinct, but similar molecules in the asymmetric unit.

this iron(II)-hydroxide were longer than in its iron(III) analogue (Table 2). The observed Fe−OH distances of 1.915 Å and 1.934 Å for the two molecules in the asymmetric unit are within the normal range of previously identified iron(II)-hydroxide species,[24,95] and the Fe−O bond elongation of 0.1 Å going from Fe(III) to Fe(II) is comparable to Borovik's tris-ureayl iron(III)/iron(II)-hydroxide pair as well as enzymatic systems (Table 3).[24,27,31,95] Taken together, the structural characterization of discrete, isolable iron(II)-triflate, iron(III)-hydroxide, and iron(II)-hydroxide units from reactions with O_2, reductants, bases, and/or acids builds a foundation for the O_2 reduction cycle mediated by the N4Py^{2R} system.

Isotope Labeling Experiments. Mass spectrometry experiments with ^{18}O-labeled dioxygen suggest inner-sphere activation and cleavage of O_2 by the hydrogen-bonded complexes **11** and **12**. A mass spectrum of synthetically prepared **13** from the reaction of **11** with $^{18}O_2$ shows about 30% incorporation of ^{18}O into the bound hydroxide group (Figure 6). We speculate that the reduced ^{18}O content in the final product was a result of exchange during the synthetic recrystallization workup and mass spectral analysis. As illustrated in Supporting Information, Figure S2, trace amounts of methanol in the mass spectrometer that had been flushed thoroughly with dry CH_3CN prior to use show rapid exchange of the labile ^{16}OH with $^{16}OCH_3$, with almost 50% exchange within 45 s. An alternative pathway could involve exchange of $H_2{}^{18}O$ with intermediates from autoxidation of **11**, but is less likely since **11** does not show readily accessible outer-sphere oxidations in acetonitrile (Supporting Information, Figure S1).

IR absorption measurements on iron(II)-hydroxide species generated from O_2 cleavage/reduction or OH^- reaction pathways with deuterated ligands suggest that the second-sphere aniline hydrogen-bond pendants participate in acid−base reactivity. We performed measurements on these reduced iron(II) species as no distinct ν(O−H) stretches are observed for the corresponding iron(III)-hydroxide complexes; the ν(O−H) signature is presumably masked by strong intramolecular hydrogen bonding (Supporting Information, Figures S3, S4, and S9).[31,39,42−44]

Using a partially deuterated ligand **10-ND** (25% deuterated at the aniline N-*H* and 85% deuterated at the methine hydrogen as determined by ^{1}H NMR spectroscopy), we prepared the corresponding iron(II)-triflate (**12-ND**) for IR studies. We observe ν(N−D) stretches at 2510 and 2425 cm^{-1}, corresponding to ν(N−H) stretches at 3395 cm^{-1} and 3290 cm^{-1}, respectively (Supporting Information, Figure S5a); quantitative information about the amount of deuterium incorporation is not available owing to the paramagnetic nature of **12-ND**. The baseline protonated iron(II)-hydroxide complex **16** exhibits distinct ν(O−H) and ν(N−H) stretches at 3670 and 3185 cm^{-1}, respectively (Supporting Information, Figure S5b). The fully deuterated iron(II)-deuteroxide complex [N4Py^{2PhND}Fe^{II}(OD)][OTf] (**16-OD**) prepared by treatment of **12** with 30% NaOD in D_2O displays a strong ν(O−D) stretch at 2705 cm^{-1} with ν(N−D) stretches at 2280 cm^{-1} and 2215 cm^{-1} (Supporting Information, Figure S5c).

The reaction of **12-ND** bearing a partially labeled N−D ligand with O_2 in CH_3CN followed by cobaltocene reduction results in a final Fe^{II}−OH/OD species with a

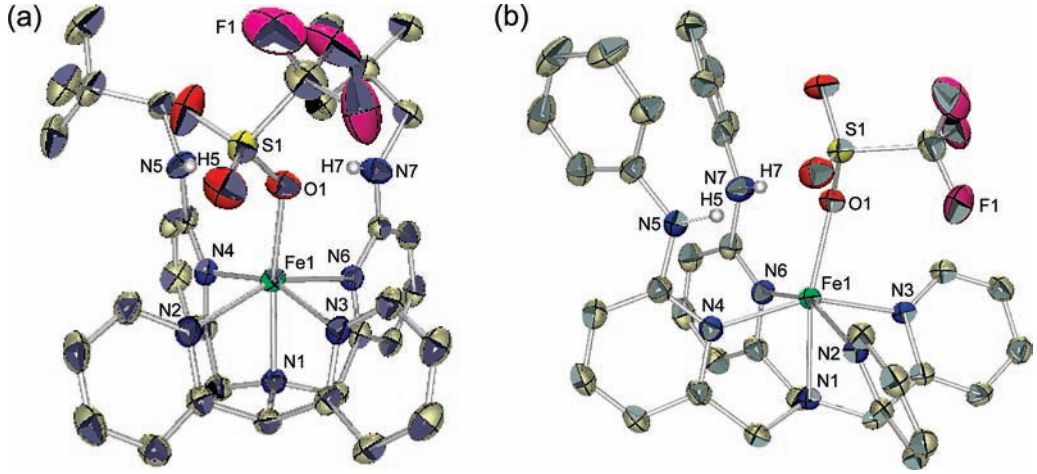

Figure 3. Solid-state structures of (a) complex **11** and (b) complex **12**. The triflate counterions and most of the hydrogens have been omitted for clarity. The H5 and H7 hydrogens on the amines have been included to highlight the hydrogen bonding interactions. The Fe, S, F, O, N, and C are shown in green, yellow, pink, red, blue, and gray, respectively, and all ellipsoids are shown at the 50% probability level.

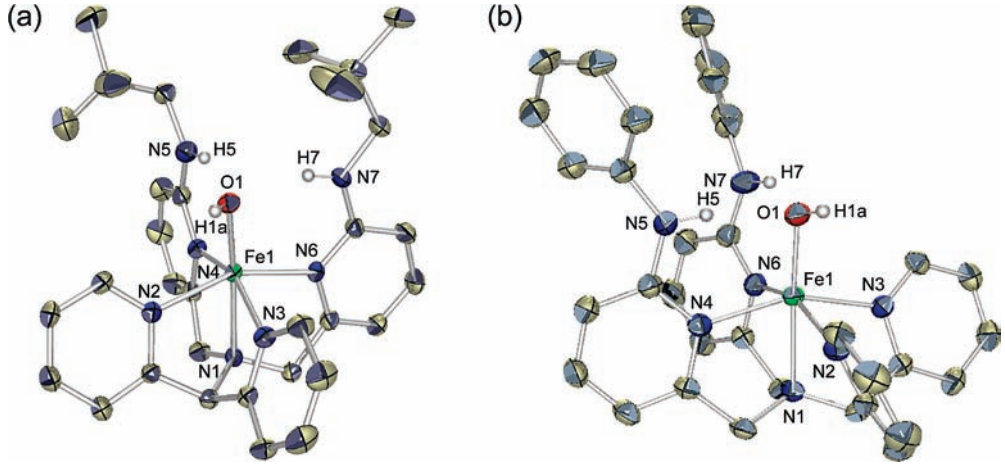

Figure 4. Solid-state structures of (a) complex **13** and (b) complex **14**. The triflate counterions, solvent molecules, and most of the hydrogens have been omitted for clarity. The H1a of the hydroxide and the H5 and H7 of the amines have been included to highlight the hydrogen bonding interactions. The Fe, O, N, and C are shown in green, red, blue, and gray, respectively, and all ellipsoids are shown at the 50% probability level.

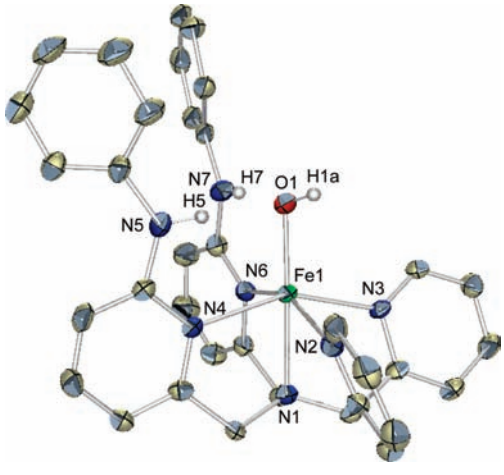

Figure 5. Solid-state structure of one of the two molecules of **16** in the asymmetric unit. The triflate counterions, solvent molecules, and most of the hydrogens have been omitted for clarity. The H1a of the hydroxide and the H5 and H7 of the amines have been included to highlight the hydrogen bonding interactions. The Fe, O, N, and C are shown in green, red, blue, and gray, respectively, and all ellipsoids are shown at the 50% probability level.

diminished ν(N−D) stretch at 2305 cm^{-1} and growth of a minor feature at 2700 cm^{-1} attributable to a ν(O−D) stretch (Supporting Information, Figure S5d), which suggests an internal HAT between the N−D group of the ligand and a higher-valent iron transient. Compared to the IR spectrum in Supporting Information, Figure S5c, which shows global deuterium incorporation into multiple parts of the ligand and therefore fewer absorptions in the 2700−3200 cm^{-1} region, the ν(O−D) feature at 2700 cm^{-1} in Supporting Information, Figure S5d is predominantly masked by the more intense N−H and C−H stretches in this region because the aniline deuterium label in **12-ND** can only be conserved or lost during workup.

Concluding Remarks

In summary, we have presented a hydrogen-bond functionalized N4Py platform that facilitates O_2 reduction in a discrete synthetic cycle by O−O activation, cleavage, and coupled electron and proton transfer. The second-sphere pendants not only turn on iron-O_2 reactivity but funnel their chemistry to structurally and spectroscopically characterized

Table 3. Comparison of Fe−O Bond Lengths (Å) for **13**, **14**, and **16** Relative to Selected Published Molecules

	Oxidation State	Fe−O (Å)
13[a]	III	1.837(3)
14[a]	III	1.835(2)
$[FeH_3buea(O)]^{2-}$[b]	III	1.813(3)
$[FeH_3buea(OH)]^{-}$[b]	III	1.926(2)
$[tpa^{Mes}Fe(OH)]^{-}$[c]	III	1.867(2)
[Fe(tnpa)(PhCOO)(OH)]$^{+}$[d]	III	1.876(2)
[(HPX-CO_2H)Fe(OH)][e]	III	1.868(3)
$[Fe0^{iPr}(OH)]^{-}$[f]	III	1.877(3)
$[FeH1^{iPr}(OH)]^{-}$[f]	III	1.8861(11)
16[a]	II	1.915(3)
		1.934(3)
$[FeH_3buea(OH)]^{2-}$[b]	II	2.048(2)

[a] This work. [b] H_3buea = tris[(*N*′-*tert*-butylureayl)-*N*-ethylene]amine.[24,27,31] [c] tpa^{Mes} = tris-mesityl tris(pyrrolylmethyl)amine.[86] [d] tnpa = tris(6-neopentylamino-2-pyridylmethyl)amine).[93] [e] HPX-CO_2H = hanging porphyrin xanthene.[94] [f] 0^{iPr} = tris[*N*-isopropylcarbamoylmethyl]aminato; $H1^{iPr}$ = [(*N*′-*tert*-butylureayl)-*N*-ethyl]-bis(*N*′′-isopropylcarbamoylmethyl)-aminato.[44]

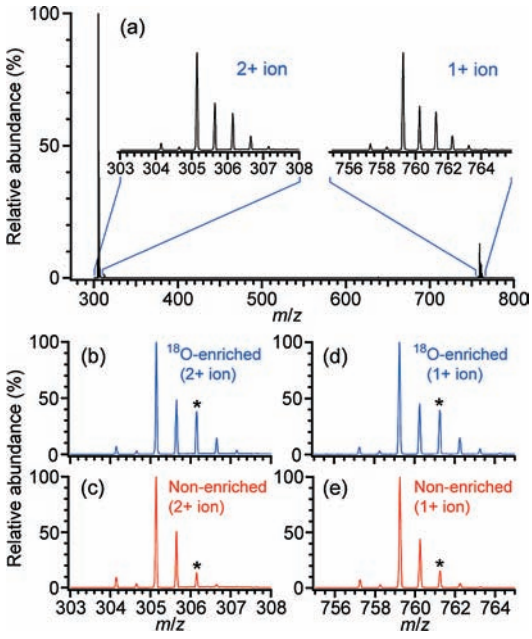

Figure 6. (a) Electrospray mass spectrum of **13-^{18}OH**, generated by reacting **11** with $^{18}O_2$, with insets showing details for the isotopic distributions of the $[N4Py^{2NpNH}Fe^{III}(OH)]^{2+}$ and $[N4Py^{2NpNH}Fe^{III}(OH)][OTf]^{+}$ ions (denoted as "2+ ion" and "1+ ion", respectively). Comparison between isotopic distributions measured for samples generated by reaction with $^{18}O_2$ (b, d) and with non-enriched O_2 (c, e). The asterisks denote the isotopic peaks at m/z = 306.15 (2+ ion) and 761.25 (1+ ion), which were measured at 38%, 13%, 40%, and 15% abundance in (b), (c), (d), and (e), respectively, relative to the most abundant isotopic peak in the distribution.

monomeric iron(III)-hydroxide products. The acid- and base-stability of the $N4Py^{2R}Fe$ system allows regeneration of the starting iron(II)-triflate complexes by electron and proton transfer to release water and complete the synthetic cycle. X-ray crystallographic characterization of the homologous iron(II)-triflate, iron(III)-hydroxide, and iron(II)-hydroxide $N4Py^{2R}$ complexes provide structural snapshots of the overall process. Mass spectrometry and infrared absorption data with various isotope labels suggest that the hydrogen-bond facilitated O_2 reduction cycle is complex. A possible scenario is that the reaction proceeds through inner-sphere O_2 binding to the labile, high-spin iron(II) center followed by O−O activation, cleavage, and hydrogen atom transfer (HAT) steps to afford monomeric iron(III)-hydroxide products that can be cycled back to the starting iron(II)-triflate complexes by electron and proton transfer.[92,96] Whereas outer-sphere oxidation of complexes **15** and **16** with AgOTf was facile (Scheme 2), the corresponding reaction with O_2 as the oxidant did not produce the counterparts **13** and **14**, since displacement of the strongly hydrogen-bonded OH^- ligand is more difficult compared to the OTf^- anion (cf. Figures 3 and 5, Table 2). Moreover, cyclic voltammetry measurements on both **11** and **12** showed no reversible or irreversible oxidative waves in the electrochemical window of CH_3CN (Supporting Information, Figure S1), precluding outer-sphere oxidations of both iron(II)-triflates by O_2. However, autoxidative reaction trajectories are difficult to rule out in these complex O_2 activation pathways; with clean isosbestic conversions of iron(II)-triflate to iron(III)-hydroxide units with no observable intermediates as monitored by UV−visible absorption changes (Figure 2), alternative approaches would be necessary to further elaborate the intricacies of this reaction pathway. We are currently pursuing further studies to understand the present O_2 reduction system as well as expanding this second-sphere approach to other small-molecule activation reactions.

Experimental Section

Synthetic Materials and Methods. Silica gel P60 (SiliCycle) and activated basic aluminum oxide (Brockmann I, 150 mesh, 58 Å, Sigma-Aldrich) were used for column chromatography. Analytical thin layer chromatography was performed using Silicycle 60 F_{254} silica gel (precoated sheets, 0.25 mm thick) and EMD Chemicals Inc. 60 F_{254} basic aluminum oxide (precoated sheets, 0.25 mm thick). Unless otherwise stated, all air-and moisture-sensitive manipulations were performed either in a Vacuum Atmospheres Company glovebox under an atmosphere of purified nitrogen or using standard Schlenk techniques. Enriched $^{18}O_2$ (97.9% enriched, >99.8% purity) was purchased from Cambridge Isotope Laboratories and used as received. Acetonitrile, dichloromethane (CH_2Cl_2), Et_2O, DME, pentane, THF, and toluene were passed through a Vacuum Atmospheres Solvent Purifier system prior to use. Acetonitrile-d_3 (Cambridge Isotope Laboratories) was refluxed over calcium hydride and distilled under dinitrogen. Celite and 4 Å molecular sieves were dried in vacuo at 160 °C. NMR chemical shifts are reported in parts per million with respect to residual protic solvent peaks; coupling constants are reported in hertz. The known compounds 2-pivaloylamido-6-methylpyridine (**1**),[82] 2-pivaloylamido-6-(bromomethyl)pyridine (**4**),[82] and di-2-pyridylmethanamine[90] were prepared by slight modification of previously reported procedures.

Instrumentation. NMR spectra were recorded using Bruker spectrometers operating at 300 or 400 MHz at room temperature as specified. UV−visible absorption spectra and kinetic runs were recorded using Varian Cary 50 UV−visible spectrophotometers, with solution samples housed in Schlenk-modified cuvettes. Cyclic voltammograms (CVs) were obtained with a BASi EC Epsilon electrochemical analyzer. Mass spectrometry and elemental analyses were performed at the QB3/Chemistry Mass Spectrometry and Microanalytical facilities, respectively, at the University of California, Berkeley. Experimental details for the mass spectrometry measurements of **13** and **13-^{18}OH** are included in a following section.

(96) Mayer, J. M. *Annu. Rev. Phys. Chem.* **2004**, *55*, 363–390.

6-Methyl-*N*-phenylpyridin-2-amine (2).[88] Freshly distilled aniline (5.56 mL, 61.3 mmol) and 2-bromo-6-methyl-pyridine (3.00 g, 17.4 mmol) were mixed together in a heavy-walled reaction flask. The resulting yellow solution was heated to 170 °C for 2 days and then cooled to room temperature. The resulting purplish-black solution was mixed with 20% aqueous NaOH (30 mL) and subsequently extracted with CH_2Cl_2 (3 × 30 mL). The purple organic layer was dried over anhydrous Na_2SO_4, and the solvent was removed to yield a purple oil. After purification by column chromatography (silica, gradient from CH_2Cl_2 to 50% CH_2Cl_2/50% EtOAc), 3.24 g (quantitative yield) of the product were obtained as yellow oil. ^{1}H NMR (400 MHz, $CDCl_3$): δ = 2.45 (s, 3 H), 6.50 (s, 1 H), 6.62 (d, J = 10.0 Hz, 1 H), 6.74 (d, J = 11.2 Hz, 1 H), 7.05 (m, 1 H), 7.31 (m, 5 H).

***tert*-Butyl 6-methylpyridin-2-yl(phenyl)carbamate (3).** Compound **2** (3.21 g, 17.4 mmol) and di-*tert*-butylcarbonate (Boc_2O) (9.52 g, 43.6 mmol) were added to a 100 mL round-bottom flask. DMAP (2.13 g, 17.4 mmol) and NEt_3 (11.7 mL, 87.2 mmol) were dissolved in CH_2Cl_2 (15 mL) and added to the reaction, and the resulting solution was refluxed for 2 days and concentrated to a brown solid after TLC analysis (silica, 4:1 hexanes:EtOAc) confirmed complete consumption of starting material. After purification by column chromatography (silica, gradient from 5% EtOAc/95% hexanes to 15% EtOAc/85% hexanes), 4.61 g (93%) of **3** were obtained as a colorless solid. ^{1}H NMR (400 MHz, $CDCl_3$): δ = 1.47 (s, 9 H), 2.49 (s, 3 H), 7.00 (d, J = 7.6 Hz, 1 H) 7.18 (m, 2 H), 7.25 (m, 2 H), 7.34 (m, 2 H), 7.58 (t, J=7.8 Hz, 1 H). HRFABMS (M^+) m/z calcd for $C_{17}H_{21}N_2O_2$ 285.1603, found 285.1599.

***tert*-Butyl 6-(bromomethyl)pyridin-2-yl(phenyl)carbamate (5).** A 250 mL 2-neck round-bottom flask was charged with **3** (4.61 g, 16.2 mmol), *N*-bromosuccinimide (NBS) (3.47 g, 19.5 mmol), and azobis(isobutyronitrile) (AIBN) (0.267 g, 1.63 mmol). CCl_4 (35 mL) was added, and the resulting mixture was sparged with N_2 for 15 min. The mixture was refluxed for 48 h under a nitrogen atmosphere, filtered, and rinsed with CH_2Cl_2 (15 mL). After purification by column chromatography (silica, 10% EtOAc/90% hexanes), 3.07 g (52%) of **5** were obtained as colorless crystals. ^{1}H NMR (400 MHz, $CDCl_3$): δ = 1.46 (s, 9 H), 4.42 (s, 2 H), 7.24 (m, 4 H), 7.34 (m, 3 H), 7.69 (t, J=10 Hz, 1 H). HRFABMS (M^+) m/z calcd for $C_{17}H_{20}N_2O_2Br_1$ 363.0708, found 363.0710.

***tert*-Butyl 6,6′-(dipyridin-2-ylmethylazanediyl)bis(methylene)-bis(pyridine-6,2-diyl)- bis(phenylcarbamate) (7).** To a 100 mL round-bottom flask was added **5** (3.07 g, 8.46 mmol), di-2-pyridylmethanamine[90] (0.681 g, 3.68 mmol), Cs_2CO_3 (7.18 g, 22.1 mmol), NaI (1.65 g, 11.1 mmol), and dry CH_3CN (12 mL). The resulting tan mixture was stirred for 24 h, filtered, rinsed with EtOAc, and the solvent was removed by rotary evaporation. After purification by column chromatography (basic alumina, gradient from 50% EtOAc/50% hexanes to 75% EtOAc/25% hexanes) 2.72 g (98%) of **7** were isolated as a brown oil. ^{1}H NMR (400 MHz, $CDCl_3$): δ = 1.44 (s, 18 H), 3.60 (s, 4 H), 5.04 (s, 1 H), 7.09 (d, J = 9.6 Hz, 4 H), 7.37 (m, 12 H), 7.52 (m, 6 H), 8.49 (d, J = 4.0 Hz, 2 H). ESI (M^+) m/z calcd for $C_{45}H_{48}N_7O_4$ 750.9, found 750.3.

6-(((Dipyridin-2-ylmethyl)((6-(phenylamino)pyridin-2-yl)methyl)-amino)methyl)-*N*-phenylpyridin-2-amine (10). A 100 mL round-bottom flask was charged with **7** (2.12 g, 3.63 mmol) at 0 °C, after which 3 M aqueous HCl (12 mL) was added. The resulting yellow solution was warmed to room temperature and stirred for 12 h. Saturated Na_2CO_3 (15 mL) was then added to give a colorless and foamy mixture. This mixture was extracted with CH_2Cl_2 (3 × 30 mL), dried over anhydrous Na_2SO_4, and the solvent was removed by rotary evaporation to yield 1.96 g (98%) of **10** as a colorless foamy product. ^{1}H NMR (400 MHz, $CDCl_3$): δ = 3.87 (s, 4 H), 5.46 (s, 1 H), 6.53 (bs, 2 H), 6.73 (d, J = 8.4 Hz, 2 H), 7.03 (t, J = 6.8 Hz, 2H), 7.09 (d, J = 7.6 Hz, 2H), 7.15 (t, J = 6.0 Hz, 2 H), 7.36 (m, 10 H), 7.67 (m, 2 H), 7.77 (d, J = 8.0 Hz, 2 H), 8.58 (d, J = 4.8 Hz, 2 H). ^{13}C NMR (400 MHz, $CDCl_3$): δ = 56.9, 71.7, 106.5, 114.0, 119.9, 122.0, 122.3, 123.9, 129.1, 136.2, 138.0, 140.8, 149.2, 155.2, 158.7, 160.3. HRFABMS (M^+) m/z calcd for $C_{35}H_{32}N_7$ 550.2719, found 550.2710.

2-Pivaloylamido-6-(bromomethyl)pyridine (4).[82] A 250 mL 2-neck round-bottom flask was charged with **1**[82] (13.38 g, 69.6 mmol), NBS (18.59 g, 104 mmol), and AIBN (1.14 g, 6.96 mmol). CCl_4 (75 mL) was added and the resulting mixture was sparged with N_2 for 15 min. The mixture was refluxed for 21 h, filtered, and rinsed with CH_2Cl_2 (30 mL). After purification by column chromatography (silica, gradient from 10% EtOAc/90% hexanes to 30% EtOAc/70% hexanes), 8.52 g (45%) of **4** were obtained as colorless solid. The identity of **4** was established by matching the ^{1}H NMR spectrum with that reported previously.[82] ^{1}H NMR (400 MHz, $CDCl_3$): δ = 1.34 (s, 9 H), 4.43 (s, 2 H), 7.15 (dd, J = 0.8, 7.6 Hz, 1 H), 7.69 (t, J = 7.6 Hz, 1 H), 8.00 (bs, 1 H), 8.19 (dd, J = 0.8, 7.6 Hz, 1 H).

***N*,*N*′-(6,6′-(Dipyridin-2-ylmethylazanediyl)bis(methylene)bis-(pyridine-6,2-diyl))bis-(*tert*-butylamide) (6).** To a 100 mL round-bottom flask was added **4** (4.90 g, 18.1 mmol), di-2-pyridylmethanamine[90] (1.67 g, 9.03 mmol), Cs_2CO_3 (11.77 g, 36.1 mmol), NaI (2.71 g, 18.1 mmol), and dry CH_3CN (10 mL). The resulting brown solution was stirred for 48 h, filtered, rinsed with EtOAc, and dried by rotary evaporation. After purification by column chromatography (basic alumina, gradient from 50% EtOAc/50% hexanes to 70% EtOAc/30% hexanes), 2.96 g (58%) of **6** were obtained as white powdery material. ^{1}H NMR (400 MHz, $CDCl_3$): δ = 1.33 (s, 18 H), 3.88 (s, 4 H), 5.36 (s, 1 H), 7.10−7.20 (m, 2 H), 7.29 (d, J = 7.6 Hz, 2 H), 7.60−7.70 (m, 6 H), 7.96 (bs, 2 H), 8.07 (d, J = 8.0 Hz, 2 H), 8.58 (m, 2 H). HRFABMS (M^+) m/z calcd for $C_{33}H_{40}N_7O_2$ 566.3243, found 566.3258.

6-((((6-Aminopyridin-2-yl)methyl)(dipyridin-23-ylmethyl)amino)-methyl)pyridin-2-amine (8). Compound **6** (1.88 g, 3.32 mmol) was dissolved in 3 M aqueous HCl (20 mL) and refluxed for 24 h. After cooling to room temperature, the pH was adjusted to > 12 with 20% aqueous NaOH (50 mL), and the aqueous phase was extracted with CH_2Cl_2 (3 × 40 mL). The combined organic phases were dried over anhydrous Na_2SO_4 and evaporated down to yield 1.11 g (79%) of **8** as white foamy material. ^{1}H NMR (400 MHz, $CDCl_3$): δ = 3.78 (s, 4 H), 4.39 (bs, 4 H), 5.42 (s, 1 H), 6.34 (d, J = 8.0 Hz, 2 H), 7.01 (d, J = 7.2 Hz, 2 H), 7.14 (t, J = 6.0 Hz, 2 H), 7.39 (t, J = 7.6 Hz, 2 H), 7.69 (m, 4 H), 8.56 (d, J = 4.8 Hz, 2 H). HRFABMS (M^+) m/z calcd for $C_{23}H_{24}N_7$ 398.2093, found 398.2105.

6-(((Dipyridin-2-ylmethyl)((6-(neopentylamino)pyridin-2-yl)-methyl)amino)methyl)-*N*-neopentylpyridin-2-amine (9). Compound **8** (0.607 g, 1.59 mmol) and trimethylacetaldehyde (0.70 mL, 6.4 mmol) were dissolved in 1,2-dichloroethane (25 mL) and stirred for 30 min at room temperature. Sodium triacetoxyborohydride (2.02 g, 9.53 mmol) was added, and the reaction mixture was stirred for a further 24 h. The reaction was quenched with 20% aqueous NaOH (20 mL) and the aqueous phase was extracted with CH_2Cl_2 (2 × 30 mL). The combined organic phases were dried over anhydrous Na_2SO_4 and evaporated down to give **9** as white foamy material in quantitative yield. ^{1}H NMR (400 MHz, $CDCl_3$): δ = 0.98 (s, 18 H), 3.04 (d, J = 6.4 Hz, 4 H), 3.75 (s, 4 H), 4.51 (t, J = 6.2 Hz, 2 H), 5.40 (s, 1 H), 6.24 (d, J = 8.4 Hz, 2 H), 6.97 (d, J = 7.2 Hz, 2 H), 7.14 (t, J = 6.0 Hz, 2 H), 7.38 (t, J = 8.0 Hz, 2 H), 7.67 (t, J = 7.4 Hz, 2 H), 7.75 (d, J = 7.6 Hz, 2 H), 8.56 (d, J=4.0 Hz, 2 H). ^{13}C NMR (400 MHz, $CDCl_3$): δ = 27.5, 32.0, 54.0, 56.7, 71.0, 103.7, 111.1, 121.8, 123.9, 136.1, 137.8, 149.2, 158.3, 159.0, 160.3. HRFABMS (M^+) m/z calcd for $C_{33}H_{44}N_7$ 538.3658, found 538.3656.

Complex 11. Ligand **9** (0.570 g, 1.06 mmol) was dissolved in DME (7 mL) and added to $Fe(OTf)_2(CH_3CN)_2$ (0.462 g, 1.06 mmol) to produce an orange solution. After 2 h, the solution was

dried in vacuo, and the orange residue was crystallized from 5 mL of DME layered beneath 10 mL of pentane. In two crops, **11** was collected as 0.600 g (63%) of yellow crystals suitable for X-ray diffraction. ^{1}H NMR (400 MHz, CD_3CN): δ = −3.30, −1.59, −0.02, 28.65, 51.53. Evans' Method μ_{eff} = 5.1 μ_B. Anal. Calcd for $C_{35}H_{43}N_7O_6F_6S_2Fe$: C, 47.14; H, 4.86; N, 11.00. Found: C, 47.04; H, 4.98; N, 10.94.

Complex 13. Complex **11** (0.198 g, 0.22 mmol) dissolved in CH_3CN (10 mL) was degassed by 3 freeze−pump−thaw cycles before excess O_2 (1 atm) was introduced at room temperature. After 16 h, the dark green solution was dried in vacuo. Recrystallization from THF (2 mL) layered below Et_2O (2 mL)/pentane (4 mL) gave **13** as 0.080 g (40%) of blue crystals, suitable for X-ray diffraction. Subsequent preparations on smaller scales provided up to 92% yields of the product. ^{1}H NMR (400 MHz, CD_3CN): δ = −4.94, 2.68, 17.39, 37.20, 88.40, 134, 159. ^{19}F NMR (400 MHz, CD_3CN): δ = −78.05. Evans' Method μ_{eff} = 5.6 μ_B. Anal. Calcd for $C_{43}H_{60}N_7O_9F_6S_2Fe$: C, 49.05; H, 5.74; N, 9.31. Found: C, 48.97; H, 5.61; N, 9.48. UV−vis: λ_{max} = 240 nm, ε = 2200 M^{-1} cm^{-1}; λ_{max} = 315 nm, ε = 1100 M^{-1} cm^{-1}; λ_{max} = 620 nm, ε = 770 M^{-1} cm^{-1}.

Complex 15. A solution of 20% aqueous NaOH (0.03 mL, 0.21 mmol) was added to **11** (0.053 g, 0.059 mmol) dissolved in THF (2 mL) under N_2. The solution gradually changed color from yellow to deep red over 1 h, after which it was dried in vacuo. The residue was extracted with CH_2Cl_2 and filtered to remove NaOTf and excess NaOH. After recrystallization from DME (2 mL) layered below pentane (6 mL), 0.028 g (63%) of the red **15** were isolated. ^{1}H NMR (400 MHz, CD_3CN): δ = 1.77, 2.31, 21.49, 29.99, 38.56, 45.91, 51.48, 60.98, 92.70, 104.38, 135.05. Evans' Method μ_{eff} = 4.7 μ_B. Anal. Calcd for $C_{34}H_{44}N_7O_4F_3SFe$: C, 53.76; H, 5.84; N, 12.91. Found: C, 53.93; H, 5.98; N, 12.79.

Regeneration of 11 from 13 and Ascorbic Acid. Complex **13** (0.364 g, 0.040 mmol) dissolved in CH_3CN (2 mL) was added to ascorbic acid (0.0035 g, 0.020 mmol) at room temperature. The dark blue solution turned green before turning yellow over 1 h as the ascorbic acid dissolved. After 2 h, the yellow solution was dried in vacuo. The ^{1}H NMR spectrum matched data obtained for **11**, synthesized independently as described above. After extracting the residue with trifluorotoluene and recrystallization from pentane, 0.0150 g (42%) of **11** was isolated. Because of possible coordination of ascorbic acid byproduct, **11** could not be isolated in higher yields after further recrystallization.

Complex 12. In a glovebox, **10** (0.500 g, 0.910 mmol) was dissolved in DME (4 mL) and added to $Fe(OTf)_2(CH_3CN)_2$ (0.397 g, 0.910 mmol) to yield an orange solution. After 1 h, the solution was dried in vacuo, and the orange residue was crystallized from DME (2 mL) layered beneath pentane (6 mL). The mother liquor was decanted to yield 0.703 g (78%) of **12** as yellow crystals suitable for X-ray diffraction. ^{1}H NMR (400 MHz, CD_3CN): δ = 0.52, 4.29, 4.72, 4.96, 5.65, 16.70, 17.19, 26.52, 32.38, 43.98, 50.00, 52.03, 62.64, 63.53. ^{1}H NMR (400 MHz, CD_2Cl_2): δ = −60.35, −9.46, −0.90, 0.76, 3.94, 4.68, 5.09, 8.44, 10.90, 16.81, 17.75, 28.00, 32.63, 49.92, 53.68, 62.32, 62.81, 63.86, 69.99, 137.49, 148.78, 150.32. Evans' Method (CD_3CN) μ_{eff} = 4.7 μ_B. Anal. Calcd for $C_{37}H_{31}N_7O_6F_6S_2Fe$: C, 49.18; H, 3.46; N, 10.85. Found: C, 49.42; H, 3.40; N, 10.87.

Complex 14. (a) With PhIO as the oxidant: **12** (0.054 g, 0.060 mmol) was dissolved in CH_3CN (5 mL) and added to PhIO (0.025 g, 0.114 mmol). The solution rapidly changed color from yellow to blue. The solution stirred for 1.5 h, filtered, and dried in vacuo. The blue residue was crystallized out of DME (2 mL) layered beneath Et_2O (2 mL)/pentane (4 mL). The mother liquor was decanted to yield 0.053 g (quantitative) of blue **14**•DME crystals suitable for X-ray diffraction. ^{1}H NMR (400 MHz, CD_3CN): δ = −5.62, 4.70, 8.85, 91.84, 137, 155. Evans' Method μ_{eff} = 5.0 μ_B. Anal. Calcd for $C_{41}H_{42}N_7O_9F_6S_2Fe$: C, 48.72; H, 4.19; N, 9.70. Found: C, 48.38; H, 4.16; N, 9.93. UV−vis: λ_{max} = 230 nm, ε = 6300 M^{-1} cm^{-1}; λ_{max} = 270 nm, ε = 7000 M^{-1} cm^{-1}; λ_{max} = 615 nm, ε = 1100 M^{-1} cm^{-1}.

(b) With O_2 as the oxidant: **12** (0.042 g, 0.046 mmol) dissolved in CD_3CN (1 mL) was concentrated in a 25 mL Schlenk tube before excess O_2 (1 atm) was introduced at room temperature. After 2 days, the deep blue solution was dried in vacuo. Repeated recrystallization from THF (1 mL) layered below Et_2O (3 mL) gave **14** as 0.031 g (73%) of blue crystals. The ^{1}H NMR spectrum and unit cell volume for the isolated compound matched data from material obtained by method (a).

(c) From **16** with AgOTf as the oxidant: A solution of AgOTf (0.0037 g, 0.014 mmol) dissolved in THF (2 mL) was added to **16** (0.011 g, 0.014 mmol) at room temperature. The reaction mixture turned purple before becoming a dark blue mixture with gray precipitate within 5 min. After 1 h, the mixture was filtered through Celite, dried in vacuo, and the residue recrystallized from THF (1 mL) and Et_2O (3 mL) to afford 0.0051 g (48%) of dark blue, microcrystalline **14**. The ^{1}H NMR spectrum and unit cell volume for the isolated compound matched the data from material obtained by method (a).

Complex 16. (a) From **12** and NaOH: A solution of 20% aqueous NaOH (0.02 mL, 0.14 mmol) was added to **12** (0.045 g, 0.058 mmol) dissolved in THF (2 mL) under N_2. The solution gradually changed color from yellow to deep red over 1 h, after which it was dried in vacuo. The residue was extracted with CH_2Cl_2 and filtered to remove NaOTf and excess NaOH. After recrystallization from THF (1 mL) layered below pentane (3 mL), 0.032 g (84%) of the red **16**, suitable for X-ray diffraction, were isolated. ^{1}H NMR (400 MHz, CD_3CN): δ = 2.11, 7.38, 7.55, 7.72, 8.36, 21.82, 29.97, 40.01, 44.64, 52.06, 59.93, 96.94, 111.41, 138.12. ^{19}F NMR (400 MHz, CD_3CN): δ = −78.09. Evans' Method μ_{eff} = 4.6 μ_B. Anal. Calcd for $C_{36}H_{32}N_7O_4F_3SFe$: C, 56.04; H, 4.18; N, 12.71. Found: C, 55.87; H, 4.12; N, 12.63.

(b) From **14** and $CoCp_2$: $CoCp_2$ (0.0039 g, 0.021 mmol) dissolved in THF (1 mL) was added to **14** (0.019 g, 0.021 mmol). The dark blue solution turned red within 1 min and was dried in vacuo after 15 min. The residue was recrystallized from THF (1 mL) layered below pentane (3 mL) to afford 0.013 g (76%) of red crystals, while the poorly soluble yellow $CoCp_2$(OTf) was filtered off. The ^{1}H NMR spectrum for the isolated material was identical to data obtained using compound synthesized by method (a).

Complex 16-OD. A solution of 30% NaOD in D_2O (0.03 mL, 0.3 mmol) was added to **12** (0.035 g, 0.039 mmol) dissolved in THF (2 mL) under N_2. The solution gradually changed color from yellow to deep red over 1 h, after which it was dried in vacuo. The residue was extracted with CH_2Cl_2 and filtered to remove NaOTf and excess NaOD. After recrystallization from CH_2Cl_2 (1 mL) layered below pentane (3 mL), 0.017 g (56%) of **16-OD** were isolated as a red microcrystalline material. This product was used for IR studies.

Complex 14-OD. A solution of AgOTf (0.0041 g, 0.016 mmol) dissolved in THF (3 mL) was added to **16-OD** (0.012 g, 0.015 mmol) at room temperature. The reaction mixture turned purple before becoming a dark blue mixture with gray precipitate within 5 min. After 1 h, the mixture was filtered through Celite, dried in vacuo, and the residue was recrystallized from THF (1 mL) and Et_2O (3 mL) to afford 0.013 g (90%) of dark blue, microcrystalline **14-OD**. This material was used for IR studies.

Regeneration of 12 from 16 and Triflic Acid (HOTf). A stock solution of 21 mM HOTf in DME (1.2 mL, 0.024 mmol) was added to **16** (0.019 g, 0.024 mmol) dissolved in DME (2 mL) at room temperature. The red solution turned yellow on complete addition of the acid. After 10 min, the yellow solution was dried in vacuo. Recrystallization from DME (1 mL) layered below pentane (3 mL) gave **12** as 0.180 g (81%) of a yellow crystalline product. The ^{1}H NMR and UV−visible absoprtion spectra matched that of **12** synthesized by an independent route.

6-(((Dipyridin-2-ylmethyl)((6-(phenylamino-D)pyridin-2-yl)-methyl)amino)methyl)-*N*-phenylpyridin-2-amine-D (10-ND). A solution of 4 M DCl in D_2O (2.5 mL) was added to **7** (0.676 g, 0.902 mmol) at room temperature. The resulting yellow solution was stirred at room temperature for 1 h. A solution of 30% NaOD in D_2O (5 mL) was then added to give a white precipitate. This mixture was extracted with $CDCl_3$ (3 × 2 mL), dried over anhydrous Na_2SO_4, and evaporated to yield 0.378 g (76%) of a colorless foamy product. ^{1}H NMR indicated that the product was only about 25% deuterated at the aniline positions. Interestingly, the methine hydrogen appeared to have been substituted with up to 85% deuterium.

Complex 12-ND. Ligand **10-ND** (0.058 g, 0.106 mmol) was dissolved in DME (5 mL) and added to $Fe(OTf)_2(CH_3CN)_2$ (0.046 g, 0.106 mmol) to yield an orange solution. After 1 h, the solution was dried in vacuo, and the orange residue was crystallized from DME (2 mL) layered beneath pentane (6 mL). The mother liquor was decanted to yield 0.066 g (69%) of **12-ND** as yellow crystals.

Electrochemical Experiments. Cyclic voltammetry measurements were carried out in a glovebox under an atmosphere of N_2 with 1 mM of **11**−**14** and 100 mM of ^{n}Bu$_4$NPF$_6$ in CH_3CN. The working electrode was a glassy carbon electrode, while the reference and auxiliary electrodes were both platinum wires. Scans were measured at 100 mV s^{-1} and only changed to 50 and 400 mV s^{-1} if the redox waves appeared quasi-reversible. For **11** and **12**, measurements were first performed in the absence of ferrocene, before ferrocene was added as the internal standard (Supporting Information, Figure S1). For **13** and **14**, measurements were first performed in the absence of cobaltocene, before cobaltocene was added as the internal standard. Cobaltocene was used instead of ferrocene because the reversible redox wave for both **13** and **14** had similar potentials as ferrocene. The potentials relative to ferrocene are 0 and −210 mV for **13** and **14**, respectively.

Mass Spectrometry Experiments. Mass spectra were acquired in the positive ion mode using a quadrupole time-of-flight (Q-Tof) mass spectrometer equipped with a Z-spray electrospray ionization (ESI) source (Q-Tof Premier, Waters, Milford, MA). Compounds **13** and the ^{18}O-enriched **13-^{18}OH** were dissolved in acetonitrile on site, withdrawn into a 250 μL Gastight syringe (Hamilton, Reno, NV), and infused into the ESI probe at a flow rate of 5 μL/min using a syringe pump. Swift and precise action during data collection was necessary to prevent degradation of **13-^{18}OH** because the OH^- ligand was found to be labile and readily exchanged with trace amounts of solvents such as methanol in the instrument. The electrospray was emitted from a stainless steel capillary with an inner diameter of 127 μm. The voltages applied to the ion source optics were adjusted for optimum desolvation and transmission of the complexes of interest, in the following order: (1) sampling cone, (2) extraction cone, and (3) ion guide. The ESI capillary voltage was subsequently adjusted to maintain ion counts below the dead-time threshold (<0.1 ions per push) to prevent spectral distortion effects due to detector saturation. The ion source parameters used for the measurements reported here were as follows: ESI capillary voltage 1.0 kV, nebulizing gas flow rate 800 L/h, sampling cone voltage 10 V, extraction cone voltage 1 V, ion guide voltage 0.1 V, source block temperature 80 °C, and nebulizing gas temperature 70 °C. Dry nitrogen (boil-off from liquid nitrogen, Praxair, Danbury, CT) was used as the nebulizing gas. No cone gas was used. The pressures in the different stages of the instrument were as follows: first pumping stage 1.2 mbar, ion transfer stage 4×10^{-4} mbar, quadrupole analyzer 2×10^{-5} mbar, argon-filled cell 8×10^{-3} mbar, and Tof analyzer 7×10^{-7} mbar. The Tof analyzer was operated in "V" mode. Under these conditions, a mass resolving power[97] of 1.0×10^4 (measured at m/z = 759) was achieved, which was more than sufficient to resolve the isotopic distributions of the singly and multiply charged ions measured in this study. This enables an ion's mass and charge to be determined independently (i.e., the charge is determined from the reciprocal of the spacing between adjacent isotope peaks in the m/z spectrum).[97] Mass spectra were accumulated over a period of 2 min. Mass calibration was performed immediately prior to measurements, using solutions of sodium formate. Mass spectra were processed using MassLynx software (version 4.1, Waters).

Infrared (IR) Spectroscopic Experiments. IR samples were prepared in a glovebox filled with N_2. Typically, about 5 mg of the sample was dissolved in CH_2Cl_2 and transferred into a solution sample holder that was equipped with KBr windows. Between 4 and 32 scans were collected, and both the ambient background and the CH_2Cl_2 spectra were subtracted from the acquired data. The samples were prepared as described in the synthetic section above unless otherwise specified. The spectra shown only include the relevant region for OH/D and NH/D stretches from 1500 to 4000 cm^{-1}. Both OH to OD shifts (ν(OH)/(ν(OD) = 1.36; calcd. = 1.37) and NH to ND shifts are observed (ν(NH)/(ν(ND) = 1.43; calcd. = 1.37). These data clearly demonstrate that the hydrogens in the second-sphere cavity can be exchanged both intra- and intermolecularly.

General Methods for X-ray Crystallography. Crystals were mounted on Kapton loops in Paratone-N hydrocarbon oil. All data collections were performed on Bruker (formerly Siemens) APEX and SMART 1000 diffractometers/CCD area detector with graphite monochromated Mo Kα radiation and equipped with low temperature apparatus. Data integration was performed using the program SAINT. Data was analyzed for agreement and possible absorption using XPREP. An empirical absorption correction based on comparison of redundant and equivalent reflections was applied using SADABS. The structures were solved within the WinGX package[98] by direct methods (SHELXS-97 and SHELXS-86) and expanded using Fourier techniques (SHELXL-97). All non-hydrogen atoms were refined anisotropically except when specified below, whereas hydrogen atoms were included in calculated positions, but were not refined. For **13**, **14**, and **16**, the hydrogens for the hydroxide groups were first located in the Fourier difference maps, before being constrained as O−H groups and were not refined as well. In the case of chiral space groups, the correct enantiomer was determined by comparison of calculated and observed Friedel pairs.

Complex **11** crystallized with an unbound molecule of triflate. The triflate anion was reasonably modeled and refined anisotropically. Compound **13** crystallized with two unbound molecules of triflate and two THF molecules. One of the triflate anions was modeled adequately, whereas the second triflate anion was disordered and refined isotropically with no restraints. One of the THF molecules was reasonably modeled, whereas the second molecule of THF was refined anisotropically over two positions. Complex **12** crystallized with an unbound molecule of triflate and a well-behaved molecule of DME. The triflate anion was disordered and modeled by refining anisotropically over two positions with restraints for the bond distances and angles. Complex **14** crystallized with two unbound molecules of triflate and a relatively well-behaved molecule of DME. One of the triflate anions was modeled adequately, whereas the second triflate anion was disordered and refined isotropically over two positions with restraints for the bond distances and angles. Complex **16** crystallized with two parent molecules in the unit cell, their associated unbound triflate molecules and a disordered molecule of CH_3CN. One triflate

(97) Marshall, A. G.; Hendrickson, C. L. *Annu. Rev. Anal. Chem.* **2008**, *1*, 579–599.

(98) Farrugia, L. J. *J. Appl. Crystallogr.* **1999**, *32*, 837–838.

anion was adequately modeled, whereas the second triflate anion was disordered and refined with restraints for the bond angles and distances. The CH_3CN was disordered with N15 occupying the inversion center and was refined isotropically without hydrogen atoms. Because of the disordered position of C73 in CH_3CN, the maximum shift/error was 0.17 after 8 least-squares refinement cycles. All the salient crystallographic data are summarized in Tables 1 and 2.

Acknowledgment. We thank the University of California, Berkeley, the Dreyfus, Beckman, Packard, and Sloan Foundations, the LBNL Chemical Sciences Division (403801), and the LBNL/DOE Helios SERC (51HE112B) for funding this work. H.S.S. thanks Dr. Frederick Hollander and Dr. Allen Oliver for advice on X-ray crystallography, as well as Prof. Robert Bergman and Mr. Shaun Wong for insightful discussions and suggestions. The mass spectrometer used in this study was acquired with support from the National Institutes of Health (1S10RR02239301).

Supporting Information Available: Experimental details of the IR spectroscopic measurements, cyclic voltammograms, and mass spectrometric studies. This material is available free of charge via the Internet at http://pubs.acs.org.